Carcinogenesis, 2019, 1–11

doi:10.1093/carcin/bgz108
Advance Access publication June 6, 2019
Original Article

ORIGINAL ARTICLE

Generation of focal mutations and large genomic deletions in the pancreas using inducible *in vivo* genome editing

Amrendra Mishra, Fatemeh Emamgholi, Zulrahman Erlangga, Björn Hartleben[1], Kristian Unger[2], Katharina Wolff, Ulrike Teichmann[3], Michael Kessel[4], Norman Woller, Florian Kühnel, Lukas E.Dow[5], Michael P.Manns, Arndt Vogel, Scott W.Lowe[6], Anna Saborowski[†] and Michael Saborowski[†,*]

Department of Gastroenterology, Hepatology, and Endocrinology and [1]Department of Pathology, Hannover Medical School, Hannover, Lower Saxony 30625, Germany, [2]Research Unit Radiation Cytogenetics, German Research Center for Environmental Health, Munich, Bavaria 85764, Germany, [3]Animal House and [4]Department for Molecular Cell Biology, Max Planck Institute for Biophysical Chemistry, Göttingen, Lower Saxony 37077, Germany, [5]Weill Cornell Graduate School of Medical Sciences, Weill Cornell Medicine, New York, NY 10021, USA and [6]Cancer Biology and Genetics Program, Sloan Kettering Institute, New York, NY 10065, USA

*To whom correspondence should be addressed. Tel: +49 511 532 0; Fax: +49 511 532 8391; Email: saborowski.michael@mh-hannover.de
†These authors contributed equally to this work.

Abstract

Beyond the nearly uniform presence of *KRAS* mutations, pancreatic cancer is increasingly recognized as a heterogeneous disease. Preclinical *in vivo* model systems exist, but with the advent of precision oncology, murine models with enhanced genetic flexibility are needed to functionally annotate genetic alterations found in the human malignancy. Here, we describe the generation of focal gene disruptions and large chromosomal deletions via inducible and pancreas-specific expression of Cas9 in adult mice. Experimental mice are derived on demand directly from genetically engineered embryonic stem cells, without the need for further intercrossing. To provide initial validation of our approach, we show that disruption of the E3 ubiquitin ligase *Rnf43* accelerates $Kras^{G12D}$-dependent tumourigenesis. Moreover, we demonstrate that this system can be used to rapidly interrogate the impact of complex cancer-associated alleles through the generation of a previously unstudied 1.2 megabase deletion surrounding the *CDKN2A* and *CDKN2B* tumour suppressors. Thus, our approach is capable of reproducibly generating biallelic and precise loss of large chromosomal fragments that, in conjunction with mutant *Kras*, leads to development of pancreatic ductal adenocarcinoma with full penetrance.

Introduction

Patients diagnosed with pancreatic ductal adenocarcinoma (PDAC) face a devastating 5-year survival rate of approximately 8% (1). Genetically engineered mouse models (GEMMs) of PDAC have both improved our understanding of the pathobiology of this deadly disease and been used as preclinical models to evaluate new therapeutic strategies. Existing models reflect predominantly only simple cancer genotypes (e.g. $Kras^{G12D}/p53^{R172H}$ (2)), yet it is increasingly evident that accurately depicting the many distinct subgroups of human PDAC will require more complex genetic approaches. Indeed, many cancer-associated genetic alterations, including focal mutations and large-scale deletions, amplifications and fusions identified through sequencing studies, remain to be tested functionally in order to delineate their impact on cancer progression and therapeutic

Received: January 24, 2019; **Revised:** May 18, 2019; **Accepted:** June 5, 2019

Abbreviations

CNA	copy number alteration
ESC	embryonic stem cell
GEMMs	genetically engineered mouse models
ICE	Inference of CRISPR Edits
IPMN	intraductal papillary mucinous neoplasms
PanINs	pancreatic intraepithelial neoplasias
PDAC	pancreatic ductal adenocarcinoma
RMCE	recombination-mediated cassette exchange
sgRNA	single guide RNA.

response. For instance, large genomic deletions encompassing the *CDKN2A/2B* locus are among the most common alterations in PDAC (3–5) with distinct therapeutic implications (6,7). Although loss of CDKN2A is undoubtedly a critical driver, these deletions include many surrounding loci which may contribute to the oncogenicity of this genomic event. The generation of homozygous genomic deletions in mice has been particularly labour intensive in traditional Cre/lox-based approaches, which require the integration of two lox-sites by homologous recombination, and subsequent repeated intercrossing to attain homozygosity. In addition, recombination efficiency decreases with genomic distance, making large homozygous deletions particularly challenging to model (8–10). As such, large deletions have remained understudied in *in vivo* models and more flexible systems are needed to model such complex alleles.

Previously, we described an embryonic stem cell (ESC)-based GEMM (GEMM-ESC) that enables the rapid generation of genetically complex transgenic animals directly from ESCs. In our earlier work, we generated ESC lines with pancreas-specific expression of Tet-regulatable, EGFP-coupled short-hairpin RNAs and a mutant *Kirsten Rat Sarcoma oncogene* (*Kras*) allele (11).

In this study, we adapted our system to exploit an inducible *in vivo* CRISPR/Cas9 approach (iCRISPR) (12) to study pancreatic carcinogenesis and sought to assess the capability of this novel platform to interrogate the impact of both single gene disruptions and large genomic deletions. We show that loss of function of the candidate cancer gene *Ring finger protein 43* (*Rnf43*) accelerates mutant Kras-driven tumourigenesis, and that large homozygous deletions of the extended *CDKN2A/2B* locus can be modelled with full penetrance.

Materials and methods

Single guide RNA design, cloning and validation

Single guide RNAs (sgRNAs) were designed using CRISPOR software (13) and inserted into the px459 vector (Addgene plasmid #62988). Efficient *in vitro* genome editing was confirmed by T7 endonuclease I assays (#M0302L; New England Biolabs, MA) according to the manufacturer's protocol. For integration into KC-RIK-ESCs, U6-sgRNA DNA fragments were subcloned into the Nsi1 site of the c3GIC9-targeting vector (Addgene plasmid #62191). Primers used in T7 endonuclease I assays and for deletion detection are listed in Supplementary Table 1 (available at *Carcinogenesis* Online).

ESC culture, recombination-mediated cassette exchange and functional characterization

ESCs were maintained in M15 + leukaemia-inhibiting factor (ESGRO-LIF, #ESG1107; Merck, Kenilworth) media as previously described (11,14). Targeting vectors were co-transfected with an FlpE recombinase encoding vector (14) into KC-RIK-ESCs cells using the Mouse Embryonic Stem Cell Nucleofector Kit (#VPH-1001; Lonza, Basel, Switzerland) and an AMAXA Nucleofector II (Lonza, Basel, Switzerland) according to the manufacturer's protocol. Following hygromycin selection (8–10 days), correct targeting was confirmed by PCR as described (11). Prior to further experiments, doxycycline (dox)-independent CRISPR/Cas9 activity was excluded in selected clones by T7 endonuclease I assay, and efficient inducible genome editing was tested *in vitro* upon electroporation of a Cre-recombinase [pPgk-Cre-bpA (pPGK-Cre), Addgene plasmid #11543] into targeted KC-RIK-ESCs, followed by a 48-hour dox treatment. mKate2 and EGFP expression was analyzed on a BD FACS LSR-II (BD Biosciences, San Jose, CA).

Animal experiments

All animal experiments were performed according to protocols approved by the local authorities (The Lower Saxony State Office for Consumer Protection and Food Safety, LAVES). The generation of the KC-RIK-ESC line has been described previously (11) (then termed 'p48 ESC line'). Chimeric mice were generated by morula injection at the Max Planck Institute for Biophysical Chemistry, Göttingen, Germany. Unless indicated otherwise, KC-RIK-sgCR8 and -sgRnf43 mice were switched to dox-enriched food (625 mg/kg, Altromin, Lage, Germany) 2 days prior to birth for a total of 14 days. All KC-RIK-sgDel-A/-B mice used to generate *Ink4a/Arf* deletions were treated with a dox-enriched diet starting at 8 weeks of age for 21 days. To minimize variability due to differences in chimerism, only animals exceeding 90% coat colour chimerism were used in the experiments. Endpoint criteria included signs of ill health and/or palpable tumours >1400 mm^3.

Haematoxylin & eosin (H&E), alcian blue staining, immunohistochemistry and western blot

H&E, alcian blue staining and immunohistochemistry were performed as previously described (11). The following antibodies were used for immunohistochemistry: anti-tRFP (11) (1:1000, #AB233-234; Evrogen, Moscow, Russia), anti-CK19 (15) (1:250, #ab133496; Abcam, Cambridge, UK), anti-GFP (11) (1:200, #2956; Cell Signalling Technology, Denver), anti-CD31 (16) (1:100, #776995; Cell Signalling Technology, Denver), anti-Ki67 (17) (1:200, #ab16667; Abcam, Cambridge, UK), anti-cleaved caspase 3 (18) (1:200, #96615; Cell Signalling Technology, Denver). MTAP antibody (1:500, #66706-I-Ig; Proteintech, Rosemont) was used for western blot. Secondary antibodies goat anti-rabbit IgG (1:500, #B2770; Life technologies, Carlsbad) and goat anti-mouse IgG-HRP (1:3000, #sc-2005; Santa Cruz Biotechnology, Dallas) were used for immunohistochemistry and western blot, respectively.

Cell lines

Tumour tissue was minced and enzymatically digested for 40 minutes in digestion solution containing 2.5 mg/ml collagenase IV (#C5138-500MG; Sigma, St. Louis) and 0.1 mg/ml DNaseI (#DN25-1G; Sigma, St. Louis) in EBSS (with Ca^{2+}/Mg^{2+}; #14155-048; Gibco, Carlsbad). The cell suspension was filtered through a 70 µm cell strainer, and cells were cultured in Dulbecco's modified Eagle's medium + 10% fetal bovine serum + penicillin/streptomycin for a minimum of seven passages. The murine pancreatic cancer cell line KPflC was a gift from Jennifer Morton and the KH2 ESC line a gift from Konrad Hochedlinger. Authentication was performed by genotyping-PCR for the transgenic alleles (last tested in May 2016 and June 2018, respectively).

Array comparative genomic hybridization

Genomic copy number alterations were determined using DNA oligo-array-based genomic hybridization (CGH) using 180k mouse arrays (#AMADID 027411; Agilent Technologies, Santa Clara). DNA was extracted using the NucleoSpin Tissue Kit (#740952.50; Macherey-Nagel GmbH, Düren, Germany) and quantified using the NanoDrop 1000 Spectrophotometer (Thermo Fisher Scientific, Waltham). Tumour DNA (250 ng) and 250 ng normal reference DNA were labelled with Cy3 and Cy5 using the CYTAG CGH labelling kit for oligo arrays (#ENZ-42671-K010; Enzo, Farmingdale) according to the manufacturer's protocol. Unincorporated nucleotides were removed from the solution using Microcon YM-30 columns (#MRCF0R030, Merck, Kenilworth) before the hybridization and washing procedure was carried out following the manufacturer's protocol. Hybridized microarray slides were scanned using a G2505C Sure Scan Microarray Scanner (Agilent Technologies, Santa Clara) followed by extraction of the raw data using the

Feature Extraction 10.7 software (Agilent Technologies, Santa Clara). Copy number alterations were identified using functions from Bioconductor R packages CGHcall and CGHregions after spatial normalization of the hybridization signals using the MANOR Bioconductor library. A detailed description of the analysis workflow can be found in Hess *et al.* (19).

Human genomic copy number data

The GISTIC calls of the genomic copy number data of the human pancreatic adenocarcinoma data set provided by The Cancer Genome Atlas consortium were downloaded from cBioPortal (http://www.cbioportal.org/, data set ID: paad tcga pan can atlas 2018, n = 183). For the calculation of copy number alteration frequencies, only GISTIC calls of −2, i.e. homozygous deletion and +2, i.e. high-level amplification were used. For visualisation, the genomic positions of genes were retrieved from Ensembl (GRCh38.p12) using functions of the biomaRt R package (20). Plotting was conducted in R using standard functions.

Statistics and tools

Survival curves were generated and analyzed using GraphPad prism 7 software (GraphPad Software; San Diego) and Mantel-Cox test. Flow cytometry data were analyzed using FlowJo (FlowJo LLC; Oregon). Indel frequency was determined with online tools at www.synthego.com (21), and statistical significance was calculated by Student's *t*-test. All images were cropped in Adobe Photoshop and assembled in Adobe Illustrator (Adobe; San Jose). Fluorescence images were merged using ImageJ (ImageJ 1.50i, NIH; Bethesda) (22). The low-magnification image shown in Figure 4E was assembled from multiple images taken by the 4 × 4 snap function in Zen2.3 pro imaging software on a Zeiss AX10 microscope (Zeiss, Oberkochen, Germany). Sequenced PCR products from deletion tumour cell lines were aligned against the expected sequence using Clustal Omega (23). Alignment results were visualized using MView (24).

Results

iCRISPR drives efficient genome editing in ESCs and in the pancreas

We previously published a GEMM-ESC platform capable of rapidly generating multi-allelic pancreatic cancer-prone mice (11,25) termed 'KC-RIK ESCs' that harbour a latent *Kras*^{lslG12D} mutant (26), a pancreas-specific, Ptf1a-promoter driven Cre-recombinase (27) and a CAGS-LSL-rtTA3-IRES-mKate2 allele (CAGS-RIK) (28) to co-express a reverse tetracycline transactivator (rtTA3) and a red fluorescent reporter, mKate2, upon Cre-mediated recombination. A Col1a1 homing cassette (CHC) downstream of the *Col1a1* gene, that integrates genetic elements *in vitro* by RMCE accounts for the genetic flexibility of the system (29) (Figure 1A). To enable inducible genome editing, we utilized the c3GIC9-targeting plasmid that encodes a TRE3G-driven EGFP-IRES-Cas9 cassette and an sgRNA under the control of a constitutive U6 promoter (Figure 1B) (12). This iCRISPR-system has been successfully used for gene editing in KH2-ESCs *in vitro* as well as in the intestine of adult mice (12,30).

To assess whether the TRE3G promoter would drive sufficient Cas9 expression in our KC-RIK-ESCs to achieve efficient gene editing, we integrated the c3GIC9 vector harbouring a control sgRNA targeting a non-genic region on mouse chromosome 8 (sgCR8) (12). Gene editing from the c3GIC9 vector has been observed in targeted ESCs in the absence of dox (12). Therefore, we first tested the targeted dox-naive KC-RIK-ESC clones for the presence of insertions and deletions (indels) by T7 endonuclease I assay. Editing of the target region was found in 7/12 ESC clones tested (Figure 1C). For further *in vitro* and *in vivo* experiments, only non-mutated ESC clones were chosen. To assess induction of EGFP-coupled Cas9 by the TRE3G promoter *in vitro* following genomic integration, we induced expression of rtTA3 (and mKate2), by nucleofecting a Cre-recombinase encoding plasmid (pPGK-Cre). Forty-eight hours after addition of dox to the cell culture medium, 72% of mKate2-positive ESCs expressed EGFP as an indicator of Cas9 induction (Figure 1E; Supplementary Figure 1, available at *Carcinogenesis* Online), and T7 assays confirmed the presence of indels on chromosome 8 (Figure 1D).

Next, we generated KC-RIK-sgCR8 mice by morula injection and, to determine the extent and pattern of TRE3G-induced EGFP-coupled Cas9-expression within the adult pancreas, kept two 9-week-old animals on dox-food for 7 days before harvest. The TRE3G promoter led to mosaic pancreatic EGFP expression (Figure 1F, GFP IHC, EGFP-negative cells marked with an asterisk). To functionally confirm the efficiency and organ specificity of CRISPR/Cas9 genome editing, we comparatively performed T7 endonuclease I assays on genomic DNA extracted from the pancreas and from the tail of these mice. CR8 cleavage was readily detected in the pancreas, but not in the corresponding tail DNA, confirming the spatial control of TRE3G driven Cas9 activation, and the 'tightness' of the TRE3G promoter (Figure 1G).

Rnf43 edited pancreata exhibit acinar-to-ductal metaplasia and pancreatic intraepithelial neoplasias but not intraductal papillary mucinous neoplasms

Loss-of-function mutations in *RNF43* have been described in multiple cancers, including gastric cancer (31,32), colorectal cancer (33,34) and cholangiocarcinoma (35). In the pancreas, both intraductal papillary mucinous neoplasm (IPMN) and PDAC harbour *RNF43* mutations in 14–38% and 5%, respectively (5,36,37). RNF43 is a ubiquitin E3 ligase that suppresses Wnt/beta-catenin signalling by promoting the degradation of Wnt ligand receptor complexes (38,39). To assess the utility of the KC-RIK-sgRNA system for testing candidate cancer genes, we inserted two different sgRNAs (sgRnf43-A and sgRnf43-B) targeting *Rnf43* into the CHC locus of KC-RIK ESCs by RMCE and screened ESC clones to exclude those with dox-independent target site alterations (Supplementary Figure 2A and B, available at *Carcinogenesis* Online). We confirmed efficient dox-dependent Cas9 expression and *Rnf43* editing (Supplementary Figure 2C and D, available at *Carcinogenesis* Online) and chose one clonal ESC line per sgRNA (KC-RIK-sgRnf43-A and -sgRnf43-B) for further experiments.

Experimental cohorts of KC-RIK-sgRnf43-A and sgRnf43-B-derived mice were generated by morula injection. KC-RIK-sgCR8 mice served as a control group. Pancreatic expression of Cas9 was initiated by feeding a dox-enriched diet for 14 days, beginning 2 days prior to birth.

Three mice were randomly selected from the KC-RIK-sgRnf43-A and -sgRnf43-B cohorts and harvested after 8–10 weeks for histological evaluation. The remaining mice were allowed to thrive until meeting endpoint criteria. In 8- to 10-week-old KC-RIK-sgRnf43 mice, we observed an admixture of normal pancreatic parenchyma, acinar-to-ductal metaplasia and early pancreatic intraepithelial neoplasias (PanINs; Supplementary Figure 2E, available at *Carcinogenesis* Online), overall similar to the pancreata from CR8 mice. Thus, at this stage, the histological changes are mainly attributable to expression of mutant Kras. Similar to the human counterparts, lesions corresponding to acinar-to-ductal metaplasia and PanINs were surrounded by a desmoplastic fibroinflammatory stroma. mKate2 expression indicated efficient recombination in the exocrine pancreas and CK19 positivity confirmed ductal differentiation in the neoplastic lesions. The stromal compartment stained negative for mKate2, suggesting that it was not derived from recombined pancreatic progenitor cells undergoing epithelial-to-mesenchymal transition (Supplementary Figure 2E, available at *Carcinogenesis*

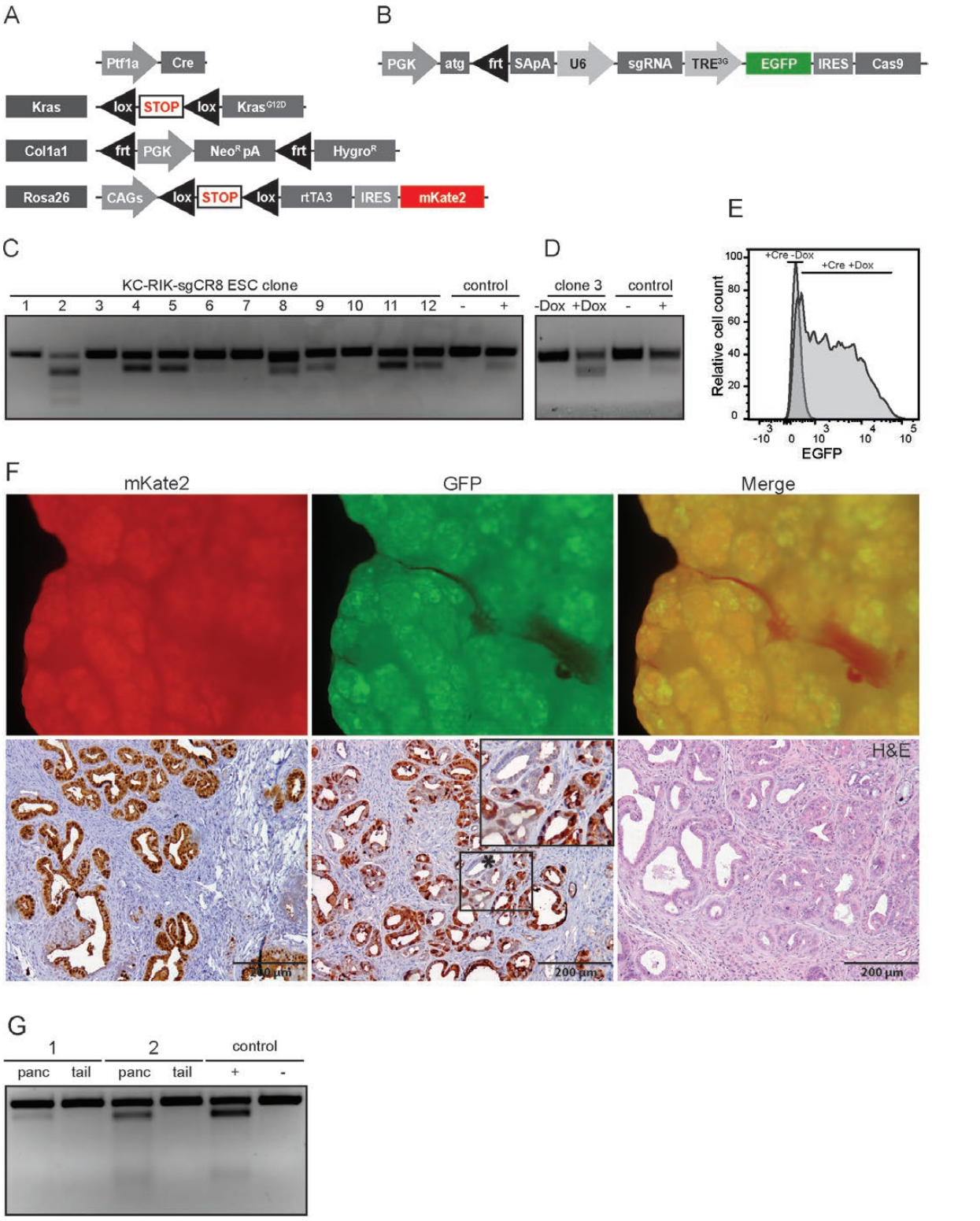

Figure 1. iCRISPR leads to efficient genome editing within the adult pancreas. **(A)** Schematic of the relevant alleles in the KC-RIK-ESCs: the pancreas-specific Ptf1a-Cre, the heterozygous *Kras*^{lslG12D} mutant within the endogenous *Kras* locus, the *Col1a1* locus harbouring the Col1a1 homing cassette (CHC) with FRT sites for recombination-mediated cassette exchange (RMCE), and the CAGS-RIK allele within the Rosa26 locus. **(B)** Schematic of the targeting vector containing an sgRNA under the control of the constitutive U6 promoter and TRE3G-driven, EGFP-coupled Cas9 (12) for RMCE-mediated integration. **(C)** Following RMCE-mediated integration of the targeting construct, ESC clones are screened for doxycycline (dox)-naive mutagenesis by T7 endonuclease I assay. Negative control: untargeted KC-RIK-ESCs; positive control: KPflC cells edited with px459-sgCR8. **(D)** T7 endonuclease I assay confirms inducible target gene editing *in vitro* in KC-RIK-sgCR8 ESCs after nucleofection with pPGK-Cre and 48 hours of doxycycline treatment. Negative control: untargeted KC-RIK-ESCs; positive control: KPflC cells edited with px459-sgCR8. **(E)** Expression of EGFP reporter in KC-RIK-sgCR8 ESCs after nucleofection with pPGK-Cre and 48 hours of doxycycline treatment. **(F)** Fluorescence images, immunohistochemistry for mKate2 and GFP and H&E stain on KC-RIK-sgCR8 pancreata. Top right corner of the GFP IHC: enlargement of the region marked with an asterisk. **(G)** T7 endonuclease I assay on genomic DNA from pancreas and corresponding tail DNA from KC-RIK-sgCR8 mice confirms genome editing in the pancreas but not in the tail. Negative control: untargeted KC-RIK-ESCs; positive control: KC-RIK-sgCR8-ESCs after nucleofection with pPGK-Cre and doxycycline treatment.

Online). Despite the recurrent loss-of-function mutations in *RNF43* in human IPMN specimens, we did not detect larger cystic lesions resembling IPMNs in the KC-RIK-sgRnf43 mice.

CRISPR-mediated disruption of Rnf43 accelerates neoplasia development and shortens survival of KC-RIK-sgRnf43 mice

KC-RIK-sgRnf43 mice exhibited a moderately reduced aggregate median survival of 228 days compared with control KC-RIK-sgCR8 mice (median survival 303 days, $P = 0.009$). Both KC-RIK-sgRnf43-A and KC-RIK-sgRnf43-B mice individually had shorter life spans compared with the controls, though only KC-RIK-sgRnf43-A mice formally reached statistical significance (214 days, $P = 0.0146$; 246 days, $P = 0.0773$, respectively; Figure 2A). Mice that reached endpoint criteria during the observation period presented with a fibrotic and largely remodelled pancreas harbouring neoplastic ductal lesions surrounded by a dense desmoplastic stroma (Figure 2E, top row). Cleavage of the target region was confirmed by T7 endonuclease I assay in pancreas biopsies (Figure 2B). Despite abundant desmoplasia, mean indel frequency across 19 pancreas biopsies reached 36.7% as determined by Inference of CRISPR Edits (ICE) analysis (21) (Figure 2C). Four out of the 14 KC-RIK-sgCR8 mice (28.6%, Figure 2D) at risk showed poorly to moderately differentiated invasive PDAC upon histological examination after harvest (Supplementary Figure 3A, available at *Carcinogenesis* Online). In the KC-RIK-Rnf43 group, the frequency of invasive PDAC (representative example in Figure 2E, bottom row) was higher compared to the KC-RIK-sgCR8 group (sgRnf43-A: 57%; sgRnf43-B: 75%; Figure 2D). Markers of proliferation, apoptosis, stromal content and vascularisation did not differ significantly between Rnf43-edited pancreata and controls (Supplementary Figure 3B–G, available at *Carcinogenesis* Online). To further assess how the editing percentage predicted by ICE analysis correlates with the relative proportion of Ptf1a-Cre recombined, mKate2 positive cells (cells at risk for Rnf43 editing) in pancreatic tumours, we stained PDAC-bearing KC-RIK-sgRnf43 pancreata for mKate2. In addition, we performed ICE analysis on consecutive tissue sections. Mean mKate2 positive area was 49.58% and corresponding ICE analysis indicated an editing efficiency of 35.89% (Supplementary Figure 3H, available at *Carcinogenesis* Online).

These results suggest that *Rnf43* is edited at high frequency in pancreata of experimental mice and, in the presence of mutant Kras, accelerates malignant progression *in vivo*.

Generation of large homozygous chromosomal deletions by dual sgRNA expression in vitro

Large genomic deletions are a frequent event in human cancers. The *INK4a/ARF* locus is located on human chromosome 9 in a genomic region that is recurrently homozygously deleted in PDAC and other cancer entities. Analysis of The Cancer Genome Atlas provisional data (http://cancergenome.nih.gov/) on 183 human pancreatic carcinoma specimens reveals that, in addition to the *INK4a/ARF* genes, several neighbouring genes are co-deleted at high frequency (Figure 3A). This region is largely syntenic between mice and humans and is located on chromosome 4 in mice (Figure 3B). The size of the genomic deletion varies between patients but frequently exceeds one megabase (Mb) (Figure 3A).

In vivo modelling of homozygous deletions using Cre/lox technology is particularly labour intensive and requires the genomic presence of four individual lox sites. CRISPR/Cas9 technology complements existing genome editing techniques and can be applied to generate deletions by tandem sgRNA expression. However, deletion frequency is inversely correlated with deletion size, and homozygous deletions exceeding 1 Mb are a particularly rare event (40). Unlike the focal genome editing that can be achieved in electroporation- or lentiviral-based systems, our inducible model is active throughout the entire pancreas. Therefore, we hypothesized that our Ptf1a-Cre-containing KC-RIK model may be particularly well suited as an experimental system for the generation of large homozygous deletions. Considering the high deletion frequency of the genomic region flanking the *INK4a/ARF* locus in pancreatic cancer, we generated sgRNAs against target sites separated by ~1.2 Mb spanning a cluster of more than a dozen genes including *Ink4a/Arf*, *Dmrta1*, *Mtap* and the *Interferon I* cluster (Figure 3B). The target sites were located in non-coding regions upstream of *Interferon B1* (sgDel-A) and downstream of *Dmrta1* (sgDel-B), respectively. Both sgRNAs were inserted into the c3GIC9 targeting vector (Figure 3C).

TRE3G-independent Cas9 expression prior to RMCE leads to cleavage of either the sgDel-A, the sgDel-B or both the sgDel-A and -B target sites in a subset of targeted and hygromycin-selected ESC clones (42.9%, $n = 14$; Supplementary Figure 4A and B, available at *Carcinogenesis* Online). Apart from chromosomal deletions following two double strand breaks, non-homologous end joining repair of each double strand break without deletion of the intervening segment is an alternative outcome of dual guide RNA expression. Supporting the assumption that local editing of an individual sgRNA target site is a more frequent event than the excision of the entire chromosomal region that requires simultaneous DNA cleavage of both guide RNA target sites, deletion detection PCR was negative in all screened clones (Figure 3D).

We chose two clones that did not exhibit cleavage at either of the two target sites for subsequent *in vitro* analysis. Following Cre-mediated activation of rtTA3 and induction of Cas9 expression by dox treatment for 48 hours, deletion-specific PCR analysis indicated the generation of deletions in both clones (Figure 3E). Sanger sequencing of the PCR-product further confirmed that the region upstream of sgDel-A was fused to the region downstream of the sgDel-B target site, resulting in the genomic excision of a ~1.2 Mb fragment *in vitro* (Figure 3F).

KC-RIK mice develop PDAC due to large chromosomal deletions on chromosome 4 with 100% penetrance

Next, we generated mice from KC-RIK-sgDel-A/B ESCs via morula injection. Starting at 8 weeks of age, mice were fed a dox-containing diet for 21 days to induce Cas9 expression. Median survival was 40 days (Figure 4A), and all mice succumbed to histologically confirmed PDAC of poor to moderate differentiation (Figure 4D, Supplementary Figure 4C, available at *Carcinogenesis* Online). Notably, several tumour foci could be detected throughout the pancreas suggesting that malignant transformation occurred not only at a single, but at multiple sites within the organ (Figure 4E). The presence of the deletion was confirmed by PCR on genomic tumour DNA (Figure 4B, top row). To determine whether loss of the extended *Ink4a/Arf* locus was a heterozygous or a homozygous event, we established cell lines from individual tumours and propagated them for at least seven passages prior to subsequent analysis in order to reduce contamination with non-tumour cells. In all tumour-derived cell lines tested ($n = 8$), deletion PCR confirmed the sustained presence of the deletion (Figure 4B, middle row), whereas inefficient

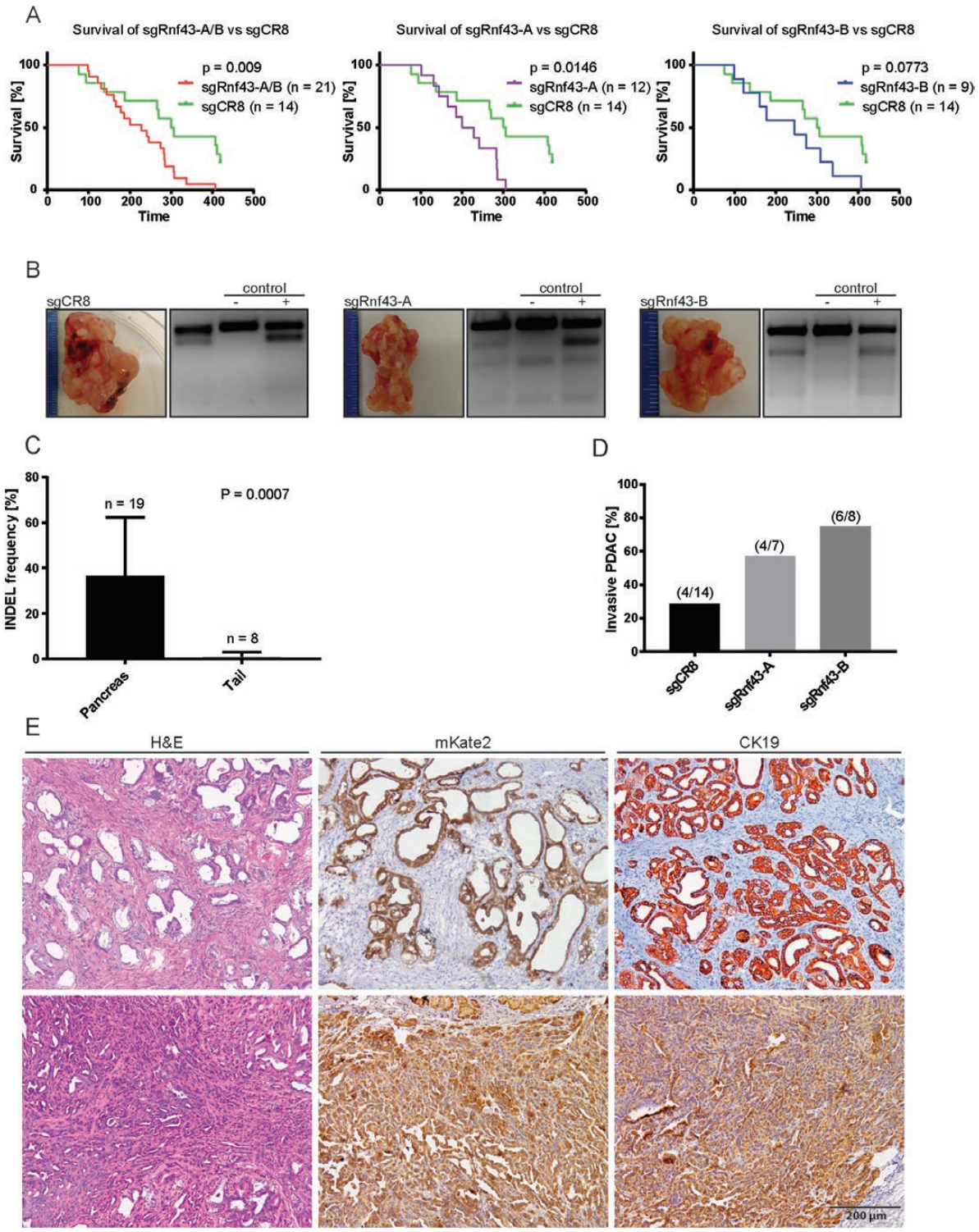

Figure 2. Intrapancreatic disruption of *Rnf43* in the presence of mutant *Kras* leads to reduced survival. **(A)** Survival of KC-RIK–sgRnf43 (-A and -B) and –sgCR8 mice. Editing of *Rnf43* leads to reduced aggregate survival of experimental mice ($P = 0.009$) compared with controls. Kaplan–Meier curves of KC-RIK–sgRnf43-A versus –sgCR8 and KC-RIK–sgRnf43-B mice versus –sgCR8 mice individually exhibit a reduced survival ($P = 0.0146$ and $P = 0.0773$, respectively. SgRnf43-A $n = 12$, sgRnf43-B $n = 9$, sgCR8 $n = 14$). **(B)** Pancreata at the time of harvest after reaching endpoint criteria. Genome editing of the targeted loci was confirmed by T7 endonuclease I assay (sgRnf43-A: 7/7, sgRnf43-B: 6/6, sgCR8: 12/12, representative examples shown). Negative control: untargeted KC-RIK-ESCs; positive control: KC-RIK-ESCs harbouring either sgCR8, sgRnf43-A or -B after nucleofection with pPGK-Cre and doxycycline treatment. **(C)** Mean indel frequency in pancreatic biopsies ($n = 19$) and tail DNA ($n = 8$) reached 36.7% and 1%, respectively, as determined by ICE analysis. **(D)** Frequency of histologically confirmed invasive PDAC assessed on a representative cross section of explanted pancreata from KC-RIK–sgCR8 (4/14), KC-RIK–sgRnf43-A (4/7) and KC-RIK–sgRnf43-B (6/8) mice. **(E)** H&E staining and immunohistochemistry for mKate2 and CK19 on two different KC-RIK-sgRnf43-A pancreata. Top row: neoplastic ductal structures surrounded by mKate2-negative stroma, resembling human PanINs. Bottom row: poorly to moderately differentiated invasive PDAC.

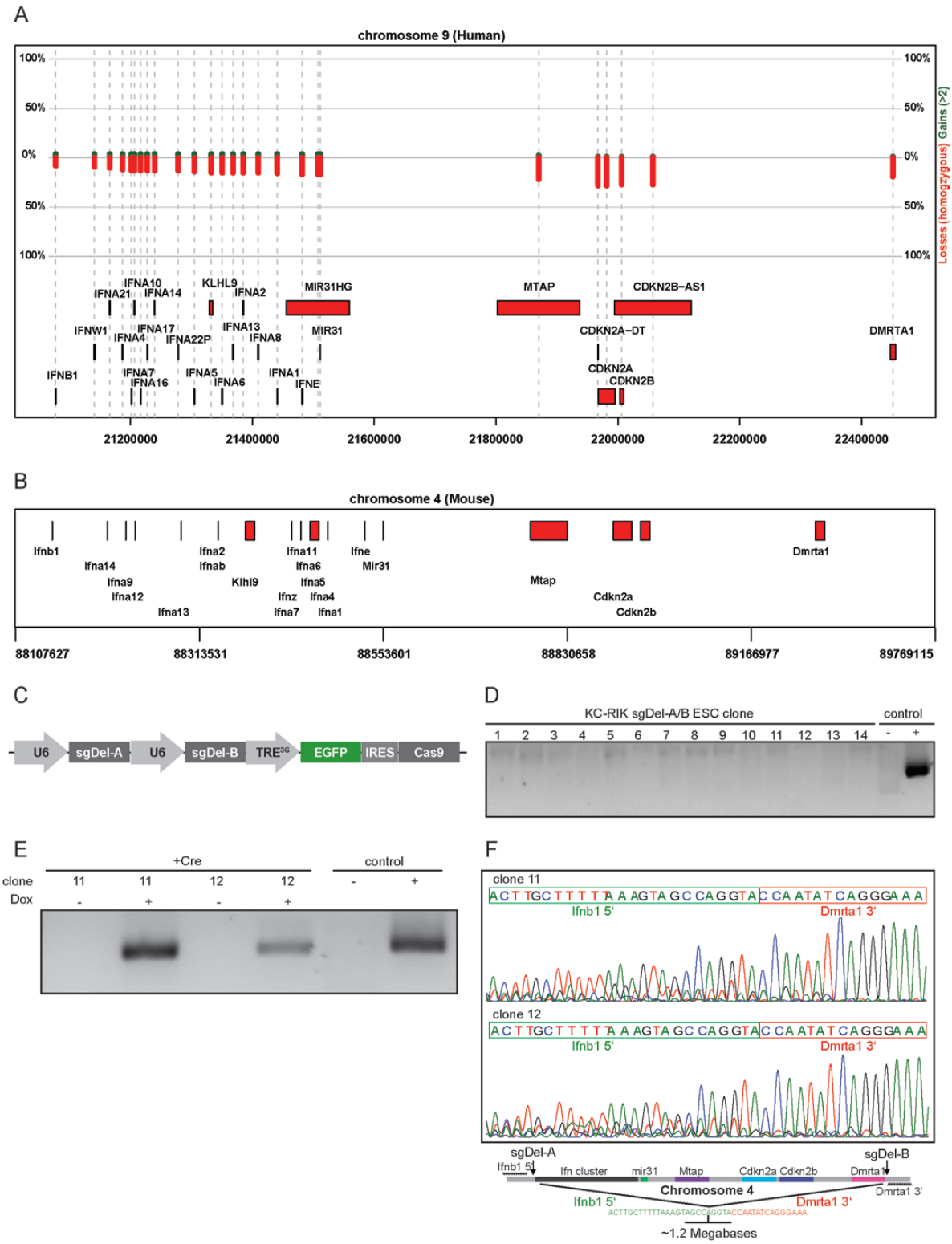

Figure 3. iCRISPR-mediated generation of a 1.2 Mb deletion in ESCs. **(A)** Schematic of the genomic region surrounding the *INK4a/ARF* genes on human chromosome 9. For each gene, the frequency of homozygous deletions or >2-fold gains is indicated in red and green vertical bars, respectively. **(B)** Schematic of the *Ink4a/Arf* locus on chromosome 4 in mice. **(C)** Schematic of the targeting vector harbouring two sgRNAs in tandem and a TRE3G-driven EGFP-IRES-Cas9. **(D)** No deletions in the doxycycline (dox)-naive ESC clones were detected by PCR using primers located 5′ of the *Ifnb1* and 3′ of the *Dmrta1* gene. Negative control: untargeted KC-RIK-ESCs; positive control: KPflC cells edited with px459-sgDel-A and px459sgDel-B. **(E)** Following electroporation of Cre recombinase and dox treatment for 48 hours, genomic deletions are readily detected by genotyping PCR. Negative control: untargeted KC-RIK-ESCs; positive control: KPflC cells edited with px459-sgDel-A and px459sgDel-B. **(F)** Sanger sequencing of the PCR product confirms fusion of the genomic region upstream of *Ifnb1* (shown in green) to the region downstream of *Dmrta1* (shown in red) using the reverse Dmrta1 3′ primer.

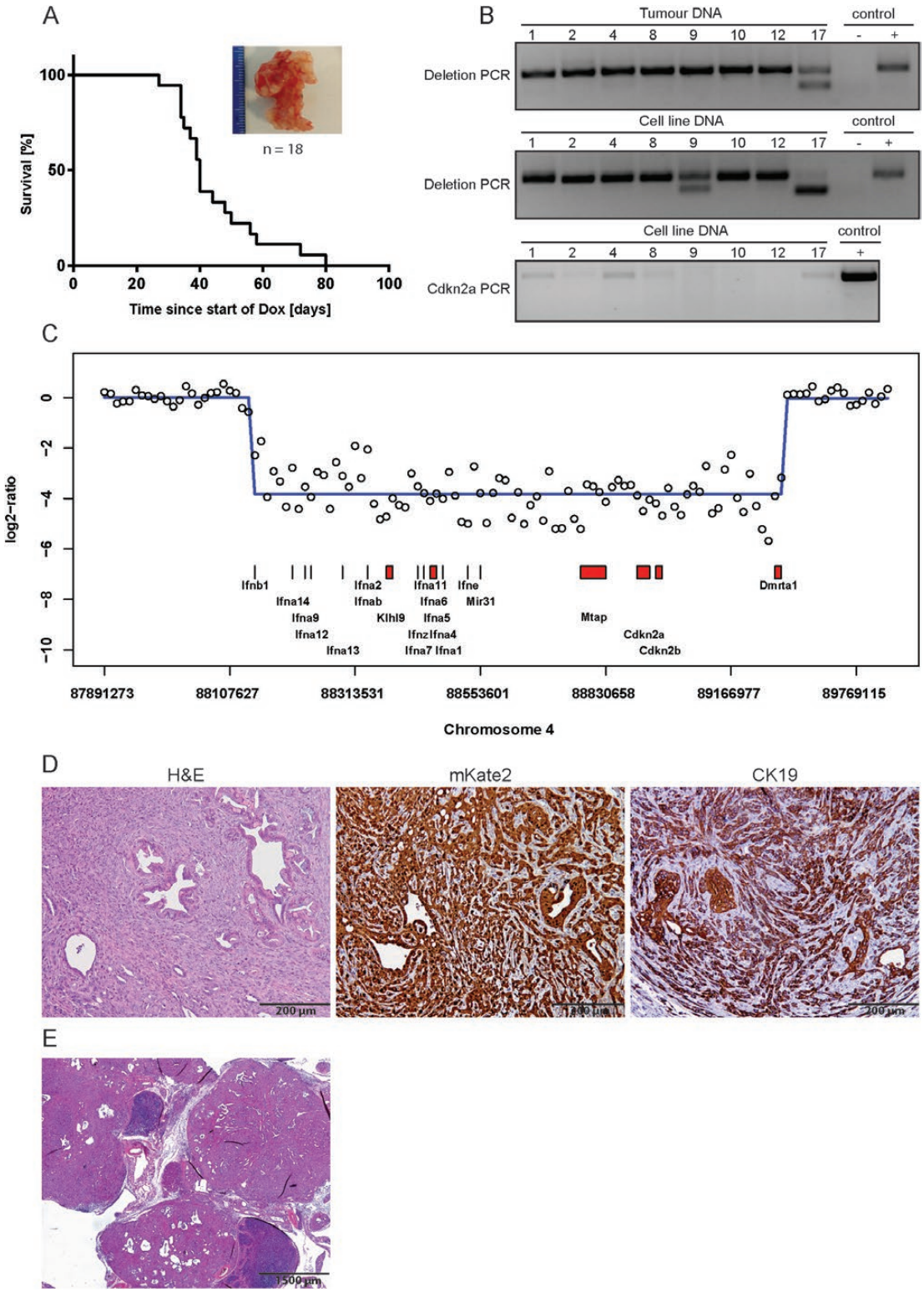

Figure 4. *In vivo* generation of an organ-specific iCRISPR-mediated homozygous large genomic deletion surrounding the *Ink4a/Arf* locus. **(A)** Survival curve of KC-RIK-sgDel-A/B mice (n = 18). X-axis indicates time after start of dox treatment. **(B)** PCR confirms the presence of the deletion in tumour DNA from eight random KC-RIK-sgDel-A/B mice, as well as in tumour - derived cell lines passaged for at least seven times. The *Ink4a/Arf* locus cannot be efficiently PCR-amplified in all cell lines tested, indicating its homozygous loss. Residual bands are likely derived from contaminating non-tumour cells. Negative control: untargeted KC-RIK-ESCs; positive control: KPflC cells edited with px459-sgDel-A and px459sgDel-B (top and middle row). Positive control: untargeted KC-RIK-ESCs (bottom row). **(C)** Representative array CGH on tumour cell line Del12 confirms that the size of the genomic deletion corresponds to the sgRNA target sites. Detailed view of the deleted region (see also Supplementary Figure 5, available at *Carcinogenesis* Online). **(D)** Representative H&E staining and immunohistochemistry for mKate2 and CK19 on one of the tumours harbouring a deletion of the extended *Ink4a/Arf* locus. Tumours were classified as poorly to moderately differentiated invasive PDAC. **(E)** H&E staining; Field image at ×5 magnification (assembly of 4 × 4 individual images) indicates the presence of multiple tumour foci within the pancreas.

PCR amplification of *Cdkn2a* on genomic DNA indicated a homozygous loss (Figure 4B, bottom row). In addition, expression of Mtap, a gene adjacent to the *Ink4a/Arf* locus, was lost as assessed by immunoblotting (Supplementary Figure 4D, available at *Carcinogenesis* Online). Further, Sanger sequencing of the PCR product spanning the deletion site confirmed the presence of the fusion event. Size variations of the PCR products are likely a consequence of variations in the exact fusion location caused by differences during the DNA repair process (Supplementary Figure 4E, available at *Carcinogenesis* Online). Successful PCR-based amplification across the fusion junction, however, neither invariably rules out the loss of larger chromosomal fragments, nor large chromosomal insertions on the second allele. Therefore, to assess whether the size of the deletion on both alleles reproducibly corresponds to the expected target sites of the two guide RNAs, we performed aCGH on our eight individually derived tumour cell lines. These arrays confirmed that on both alleles, the deletion corresponds to the intended target sites on chromosome 4, spanning the ~1.2 Mb starting upstream the *Ifnb1* gene and extending to the region downstream of the *Dmrta1* gene (Figure 4C; Supplementary Figure 5, available at *Carcinogenesis* Online). aCGH further revealed that, except for the engineered deletion on chromosome 4, each tumour exhibited a unique profile with no recurrent additional events and only small chromosomal gains and losses, reflective of an overall low genomic instability commonly observed in murine tumours (Supplementary Figure 6, available at *Carcinogenesis* Online).

Considering that loss of *INK4a/ARF* is a frequent event also in other cancer entities apart from pancreatic cancer, we reasoned that potential leakiness of our system might lead to malignant transformation within other organ systems. Both the liver and the lung were screened for neoplastic lesions, but no mKate2-positive nodules could be detected outside of the pancreas, thereby validating the robust organ specificity of our approach (Supplementary Figure 7, available at *Carcinogenesis* Online). Thus, the GEMM-ESC-based KC-RIK-tandem guide RNA approach is a highly tractable tool to efficiently model large homozygous deletions with full penetrance *in vivo*.

Discussion

GEMM-ESC-based murine models are a rapid mouse modelling platform that combines the advantages of traditional transgenic approaches with great genetic and functional flexibility. We have previously incorporated inducible RNA interference technology into GEMM-ESC models to study the consequences of downregulating or reactivating the expression of cancer-relevant genes in PDAC (11). In recent work, we used this model to delineate that the switch/sucrose nonfermeting complex member Arid1a functions as a potent regulator of Kras-induced changes in acinar cell identity (25).

CRISPR/Cas9 technology is a potent tool for genome editing applications owing to the flexibility with which it can be adapted to different genomic targets and delivery systems (41). Unlike the knockdown phenotypes generated by RNAi, CRISPR/Cas9-mediated genome editing can select for a complete loss-of-function phenotype in mice when studying cancer genes.

Here, we demonstrate that transgenic iCRISPR technology in the pancreas serves as a powerful tool not only to validate novel cancer genes, but also to generate large homozygous chromosomal deletions with high penetrance and reliable organ-specificity *in vivo*. The use of iCRISPR in genetically engineered ESCs offers multiple advantages: The dual reporter system facilitates the tracing of relevant cell populations *in vivo*: In the presence of dox, the green fluorescent reporter EGFP is expressed as a surrogate for Cas9 induction. As the Ptf1a-promoter-driven Cre-recombinase not only activates the mutant *Kras* allele but also the mKate2-encoding CAGS-RIK, cells at risk for neoplastic transformation can be readily detected amongst non-cancerous tissues such as stromal cells or immune cell infiltrates. Timed induction of Cas9 expression by administration of a dox-enriched diet facilitates genome editing at various steps of pancreas development or malignant transformation, and temporally uncouples CRISPR-induced secondary genetic events from activation of mutant *Kras*. In addition, transient Cas9 expression by dox removal likely reduces off-target effects of the CRISPR/Cas9 system.

In this work, we demonstrate how transgenic iCRISPR technology can be utilized to functionally investigate putative cancer driver genes *in vivo*. Recent data indicate that the RING finger protein *Rnf43* has tumour suppressive functions in experimental models of gastric cancer and colorectal cancer (32,33). Loss-of-function mutations in *RNF43* occur in 5% of pancreatic cancer specimens (5). In our mouse model, pancreatic loss of Rnf43 cooperates with mutant Kras to accelerate tumourigenesis and moderately reduces overall survival. *RNF43* is also mutated in 14–38% of human IPMNs (36,37), a group of pancreatic cystic lesions at risk for neoplastic transformation. Notably, in the murine system, we histologically did not detect the typical cystic appearance of IPMNs, suggesting that in our model mutant Kras/Rnf43-mediated PDAC development proceeds through precursor lesions such as acinar-to-ductal metaplasias/PanINs. Although the majority of *Rnf43*-edited pancreata harboured invasive PDAC, a subset of mice across all experimental groups exhibited a fibrotic and largely remodelled pancreas with PanIN lesions surrounded by a dense desmoplastic stroma when reaching endpoint criteria. Massive remodelling can lead to a shortage of functional pancreatic tissue, resulting in pancreatic exocrine insufficiency (25), which we assume to be the cause of non-tumour-related death in non-PDAC-bearing mice.

Synchronous expression of two sgRNAs targeting two chromosomal loci can result in the relatively rare event that the intervening DNA segment is deleted. Indeed, tandem CRISPR/Cas9 approaches have been used to create gene fusions *in vitro* and *in vivo* in the lung (42–44), the intestine (30) and in the liver (45). Most of these fusions, however, are heterozygous, and large homozygous deletions are particularly challenging to model *in vivo* because they require the bi-allelic excision of two large genomic fragments. Recently, Canver *et al.*(40) assessed the efficiency with which genomic deletions are generated by introduction of two guide RNAs *in vitro* and experimentally confirmed a strong inverse relationship between the deletion size and frequency. In more than 500 individual clonal lines harbouring one of three pairs of sgRNAs with intervening DNA segments between 70 kb and 1 Mb, no homozygous deletion was detectable in any of the clones (40).

Using transgenic and inducible CRISPR technology expressed from the CHC locus, we have shown that a large homozygous deletion of more than 1 Mb surrounding the *Ink4a/Arf* locus can be generated and lead to tumour development with complete penetrance. Experimental evidence indicates that efficient deletion of DNA fragments using CRISPR/Cas9 is sensitive to sgRNA/Cas9 dose (40). In our system, the robust and timed expression from a defined genomic locus reliably secures the controlled delivery of Cas9 and sgRNA without the risk of uncontrolled genome editing caused by continuous Cas9 expression. Multiple distinct tumour foci within the pancreata of experimental mice imply that numerous successful fusion events occurred. The

Ptf1a-Cre activates the iCRISPR-system in the vast majority of exocrine pancreatic cells. Therefore, although the generation of a large chromosomal deletion may be a rare genetic event at the cellular level, the sheer abundance of targetable cells and the robust and timed expression of Cas9 permits the reliable manifestation of the fusion phenotype, indicating that our model is well suited to study positively selected rare genetic events. aCGH confirmed the precision with which excision at the expected loci is accomplished and ruled out unwanted loss of additional chromosomal material.

Other elegant means of locoregional sgRNA delivery to the pancreas such as lentiviral-based methods (46) exist and have been used to edit individual genes. In contrast to the transient expression of CRISPR/Cas9 from the CHC locus, lentiviral insertion bears the risk of causing insertional mutagenesis, which may confound the phenotypic analysis. Focal delivery of transiently expressed Cas9 and sgRNAs by pancreas electroporation abrogates the risk of insertional mutagenesis, but efficiently transfects only a few hundred cells (47,48). The presence of only a few genetically modified cells is likely not sufficient for the reliable phenotypic manifestations of particularly rare events, including homozygous fusions.

In summary, the strength of the GEMM-ESC approach in combination with the iCRISPR technology lies in the genetic flexibility of the system, the temporal control of organ-specific genetic alterations, as well as in the continuous presence of numerous genetically modified cells, thus enabling the rapid phenotypic and functional characterization of positively selected rare genetic events.

Supplementary material

Supplementary data are available at *Carcinogenesis* online.

Funding

German Cancer Aid (111757 to M.S.); German Research Foundation (SA 2862/1-1 to M.S.); Else Kröner-Fresenius Foundation (2015_A225 to A.S.); SFB/TR 209 (to A.V., A.S., and M.S.).

Acknowledgements

We thank Sandra Rohrmoser, Eric Jende and Meriame Nassiri for their expert technical assistance. Results shown here are in part based upon data generated by the The Cancer Genome Atlas Research Network: http://cancergenome.nih.gov/.
Conflict of Interest Statement: S.W.L. is a founder, shareholder and advisory board member of Mirimus, Inc. L.E.D. is a shareholder and advisory board member of Mirimus, Inc.

References

1. Siegel, R.L. *et al.* (2018) Cancer statistics, 2018. CA. Cancer J. Clin., 68, 7–30.
2. Hingorani, S.R. *et al.* (2005) Trp53R172H and KrasG12D cooperate to promote chromosomal instability and widely metastatic pancreatic ductal adenocarcinoma in mice. Cancer Cell, 7, 469–483.
3. Cancer Genome Atlas Research Network. (2017) Integrated genomic characterization of pancreatic ductal adenocarcinoma. Cancer Cell, 32, 185–203 e13.
4. Waddell, N. *et al.*; Australian Pancreatic Cancer Genome Initiative. (2015) Whole genomes redefine the mutational landscape of pancreatic cancer. Nature, 518, 495–501.
5. Bailey, P. *et al.*; Australian Pancreatic Cancer Genome Initiative. (2016) Genomic analyses identify molecular subtypes of pancreatic cancer. Nature, 531, 47–52.
6. Mavrakis, K.J. *et al.* (2016) Disordered methionine metabolism in MTAP/CDKN2A-deleted cancers leads to dependence on PRMT5. Science, 351, 1208–1213.
7. Kryukov, G.V. *et al.* (2016) MTAP deletion confers enhanced dependency on the PRMT5 arginine methyltransferase in cancer cells. Science, 351, 1214–1218.
8. Liu, Y. *et al.* (2016) Deletions linked to TP53 loss drive cancer through p53-independent mechanisms. Nature, 531, 471–475.
9. Liu, P. *et al.* (1998) Embryonic lethality and tumorigenesis caused by segmental aneuploidy on mouse chromosome 11. Genetics, 150, 1155–1168.
10. Zheng, B. *et al.* (2000) Engineering mouse chromosomes with Cre-loxP: range, efficiency, and somatic applications. Mol. Cell. Biol., 20, 648–655.
11. Saborowski, M. *et al.* (2014) A modular and flexible ESC-based mouse model of pancreatic cancer. Genes Dev, 28, 85–97.
12. Dow, L.E. *et al.* (2015) Inducible *in vivo* genome editing with CRISPR-Cas9. Nat. Biotechnol., 33, 390–394.
13. Haeussler, M. *et al.* (2016) Evaluation of off-target and on-target scoring algorithms and integration into the guide RNA selection tool CRISPOR. Genome Biol., 17, 148.
14. Dow, L.E. *et al.* (2012) A pipeline for the generation of shRNA transgenic mice. Nat. Protoc., 7, 374–393.
15. Alba-Castellón, L. *et al.* (2016) Snail1-dependent activation of cancer-associated fibroblast controls epithelial tumor cell invasion and metastasis. Cancer Res., 76, 6205–6217.
16. Saborowski, A. *et al.* (2019) Murine liver organoids as a genetically flexible system to study liver cancer *in vivo* and *in vitro*. Hepatol. Commun., 3, 423–436.
17. Jeong, S.H. *et al.* (2018) Hippo-mediated suppression of IRS2/AKT signaling prevents hepatic steatosis and liver cancer. J. Clin. Invest., 128, 1010–1025.
18. Endig, J. *et al.* (2016) Dual role of the adaptive immune system in liver injury and hepatocellular carcinoma development. Cancer Cell, 30, 308–323.
19. Hess, J. *et al.* (2011) Gain of chromosome band 7q11 in papillary thyroid carcinomas of young patients is associated with exposure to low-dose irradiation. Proc. Natl. Acad. Sci. USA, 108, 9595–9600.
20. Durinck, S. *et al.* (2009) Mapping identifiers for the integration of genomic datasets with the R/Bioconductor package biomaRt. Nat. Protoc., 4, 1184–1191.
21. Hsiau, T. *et al.* (2018) Inference of CRISPR Edits from Sanger Trace Data. bioRxiv, 251082. doi: 10.1101/251082.
22. Schneider, C.A. *et al.* (2012) NIH Image to ImageJ: 25 years of image analysis. Nat. Methods, 9, 671–675.
23. Li, W. *et al.* (2015) The EMBL-EBI bioinformatics web and programmatic tools framework. Nucleic Acids Res., 43(W1), W580–W584.
24. Brown, N.P. *et al.* (1998) MView: a web-compatible database search or multiple alignment viewer. Bioinformatics, 14, 380–381.
25. Livshits, G. *et al.* (2018) Arid1a restrains Kras-dependent changes in acinar cell identity. Elife, 7, 1–28.
26. Jackson, E.L. *et al.* (2001) Analysis of lung tumor initiation and progression using conditional expression of oncogenic K-ras. Genes Dev, 15, 3243–3248.
27. Kawaguchi, Y. *et al.* (2002) The role of the transcriptional regulator Ptf1a in converting intestinal to pancreatic progenitors. Nat. Genet., 32, 128–134.
28. Dow, L.E. *et al.* (2014) Conditional reverse tet-transactivator mouse strains for the efficient induction of TRE-regulated transgenes in mice. PLoS One, 9, e95236.
29. Beard, C. *et al.* (2006) Efficient method to generate single-copy transgenic mice by site-specific integration in embryonic stem cells. Genesis, 44, 23–28.
30. Han, T. *et al.* (2017) R-Spondin chromosome rearrangements drive Wnt-dependent tumour initiation and maintenance in the intestine. Nat. Commun., 8, 15945.
31. Min, B.H. *et al.* (2016) Dysregulated Wnt signalling and recurrent mutations of the tumour suppressor RNF43 in early gastric carcinogenesis. J. Pathol., 240, 304–314.
32. Neumeyer, V. *et al.* (2019) Loss of endogenous RNF43 function enhances proliferation and tumour growth of intestinal and gastric cells. Carcinogenesis 40, 551–559.

33. Eto, T. *et al.* (2018) Impact of loss-of-function mutations at the RNF43 locus on colorectal cancer development and progression. J. Pathol., 245, 445–455.
34. Giannakis, M. *et al.* (2014) RNF43 is frequently mutated in colorectal and endometrial cancers. Nat. Genet., 46, 1264–1266.
35. Jusakul, A. *et al.* (2017) Whole-genome and epigenomic landscapes of etiologically distinct subtypes of cholangiocarcinoma. Cancer Discov., 7, 1116–1135.
36. Amato, E. *et al.* (2014) Targeted next-generation sequencing of cancer genes dissects the molecular profiles of intraductal papillary neoplasms of the pancreas. J. Pathol., 233, 217–227.
37. Springer, S. *et al.* (2015) A combination of molecular markers and clinical features improve the classification of pancreatic cysts. Gastroenterology, 149, 1501–1510.
38. Hao, H.X. *et al.* (2012) ZNRF3 promotes Wnt receptor turnover in an R-spondin-sensitive manner. Nature, 485, 195–200.
39. Koo, B.K. *et al.* (2012) Tumour suppressor RNF43 is a stem-cell E3 ligase that induces endocytosis of Wnt receptors. Nature, 488, 665–669.
40. Canver, M.C. *et al.* (2014) Characterization of genomic deletion efficiency mediated by clustered regularly interspaced short palindromic repeats (CRISPR)/Cas9 nuclease system in mammalian cells. J. Biol. Chem., 289, 21312–21324.
41. Ventura, A. *et al.* (2018) Modeling cancer in the CRISPR era. Ann. Rev. Cancer Biol., 2, 111–131.
42. Blasco, R.B. *et al.* (2014) Simple and rapid *in vivo* generation of chromosomal rearrangements using CRISPR/Cas9 technology. Cell Rep., 9, 1219–1227.
43. Maddalo, D. *et al.* (2014) *In vivo* engineering of oncogenic chromosomal rearrangements with the CRISPR/Cas9 system. Nature, 516, 423–427.
44. Choi, P.S. *et al.* (2014) Targeted genomic rearrangements using CRISPR/Cas technology. Nat. Commun., 5, 3728.
45. Kastenhuber, E.R. *et al.* (2017) DNAJB1-PRKACA fusion kinase interacts with β-catenin and the liver regenerative response to drive fibrolamellar hepatocellular carcinoma. Proc. Natl. Acad. Sci. USA, 114, 13076–13084.
46. Chiou, S.H. *et al.* (2015) Pancreatic cancer modeling using retrograde viral vector delivery and *in vivo* CRISPR/Cas9-mediated somatic genome editing. Genes Dev, 29, 1576–1585.
47. Maresch, R. *et al.* (2016) Multiplexed pancreatic genome engineering and cancer induction by transfection-based CRISPR/Cas9 delivery in mice. Nat. Commun., 7, 10770.
48. Gürlevik, E. *et al.* (2016) Administration of gemcitabine after pancreatic tumor resection in mice induces an antitumor immune response mediated by natural killer cells. Gastroenterology, 151, 338–350.e7.